Silicon quantum dots embedded in a SiO₂ matrix: From structural study to carrier transport properties

Nuria Garcia-Castello,[1,*] Sergio Illera,[1] Roberto Guerra,[2] Joan Daniel Prades,[1] Stefano Ossicini,[2] and Albert Cirera[1]

[1]*MIND-IN²UB, Departament of Electronics, Universitat de Barcelona, C/Martí i Franquès 1, E-08028 Barcelona, Spain*
[2]*Dipartimento di Scienze e Metodi dell'Ingegneria and Centro Interdipartimentale En&Tech, Università di Modena e Reggio Emilia, via Amendola 2 Pad. Morselli, I-42122 Reggio Emilia, Italy*

We study the details of electronic transport related to the atomistic structure of silicon quantum dots embedded in a silicon dioxide matrix using *ab initio* calculations of the density of states. Several structural and composition features of quantum dots (QDs), such as diameter and amorphization level, are studied and correlated with transport under transfer Hamiltonian formalism. The current is strongly dependent on the QD density of states and on the conduction gap, both dependent on the dot diameter. In particular, as size increases, the available states inside the QD increase, while the QD band gap decreases due to relaxation of quantum confinement. Both effects contribute to increasing the current with the dot size. Besides, valence band offset between the band edges of the QD and the silica, and conduction band offset in a minor grade, increases with the QD diameter up to the theoretical value corresponding to planar heterostructures, thus decreasing the tunneling transmission probability and hence the total current. We discuss the influence of these parameters on electron and hole transport, evidencing a correlation between the electron (hole) barrier value and the electron (hole) current, and obtaining a general enhancement of the electron (hole) transport for larger (smaller) QD. Finally, we show that crystalline and amorphous structures exhibit enhanced probability of hole and electron current, respectively.

I. INTRODUCTION

Low-dimensional structures such as quantum dots (QDs), nanowires, or thin layers embedded in an insulator matrix have recently opened a new branch of electronic technology due to the new physical properties that they exhibit. The spatial confinement in QDs helps to overcome the Shockley-Queisser limit,[1,2] i.e., the maximum theoretical efficiency of optoelectronic devices. The energy gap of the semiconductor QDs is strongly dependent on the QD diameter[3] and discrete energy states also appear inside the wide band gap of the insulator matrix, making possible tunable band gap devices.

The properties of the confinement effect and the improvement of light conversion efficiency[4] are used in a wide range of applications, such as single-electron devices,[5] new memory concepts,[6] and optoelectronic devices such as tandem solar cells[7,8] or photon-electroluminescent devices.[9,10] In this context, silicon quantum dots (SiQDs) embedded in an insulating matrix represent the most prevalent nanoscale silicon systems.[7,11–15] These works show that their effective use in a nanodevice requires a detailed knowledge of both structural and optoelectronic properties and the characteristics of device response under nonequilibrium conditions, i.e., when a bias voltage is applied or under illumination. Different structural models have been proposed to describe SiQDs and optical, structural, and electrical properties have been widely reported using density functional theory (DFT).[16–23]

From a fundamental point of view many novel electronic transport phenomena have been discovered, such as a staircase-like current-voltage (*I-V*) characteristic,[24] Coulomb blockade oscillation,[25] negative differential resistance,[4,26] or the Kondo effect.[27] Researchers have mostly concentrated on the study of single and two QDs using the nonequilibrium Green's functions formalism (NEGFF)[26,28–30] with one level of energy and constant transition rates. Arbitrary arrays of QDs are still

a challenge. To our knowledge, the unique computations of transport in an extended array have been done by Carreras *et al.*,[9] which use a semiempirical tunneling current model, by Han *et al.*[31] and Aeberhard *et al.*[32] employing one energy level per QD and NEGFF, by Taranko *et al.*[33] using one energy level per QD and the equation of motion method, and by Illera *et al.*[34,35] In the latter work,[35] we proposed a model based on the transfer Hamiltonian approach and noncoherent rate equations in order to study the electronic transport in the self-consistent field regime. In spite of its simplicity, this model can efficiently provide results similar to those obtained with more complex formalisms.[28] As a matter of fact, the effect of the local potential due to QD self-charge is included in this model and it allows one to use more than one state per QD. In particular the code can use a density of states (DOS) computed by *ab initio* calculations, which is a difficult issue to treat with NEGFF. Moreover, the proposed model can be efficiently coded in order to allow the computation of arbitrary arrays of multiple QDs.[36] This can be simply done within the adopted formalism by taking into account the capacitive coupling and the transmission coefficients between the QDs.

A common way of introducing the embedded SiO₂ matrix effect in the study of the transport between SiQDs is by using the bulk Si energy band gap and the values for tunneling barriers of the planar Si/SiO₂ heterojunction, i.e., ultrathin gate oxides in CMOS,[9] which are very close to the bulk value of the Si/SiO₂ interface.[4,8,37,38] However, such method does not take into account, among other properties, the effect of quantum confinement (QC) on the QD.[3] To our knowledge, at present there are no other theoretical studies dealing with SiQD transport properties including their intrinsic electronic structure.

Apart from the fully atomistic approach adopted in this paper, another way to obtain the DOS of SiQDs embedded in

an insulator matrix is by modeling them as a superlattice of cubic[39] or spherical[36] quantum wells with a width corresponding to the QD diameter and the above-mentioned barrier height values, i.e., the one of the planar Si/SiO₂ heterojunction for all QD sizes. With this *ab initio* study we are able to describe the structural details, such as stress or oxidation state, of the surrounding matrix in the QD energy levels. We have found that not only the positions of the discrete energy states of the QD vary with its size, but also the position of the silica band edge, which reaches the bulk value for QDs bigger than 2 nm of diameter. Therefore, the approximation of using the same barrier height for all QD sizes that can be found in the literature may hold only for QDs of large diameters.

In the present paper, we use *ab initio* ground state properties to describe realistic transmission coefficient for transport through one SiQD in contact with two semi-infinite metallic electrodes. This is performed by using the DOS of a QD inside a SiO₂ matrix in the transfer Hamiltonian formalism.[40,41] In this framework we study the dependence of the *I-V* characteristic on the QD diameter and on the amorphization level (crystalline or amorphous systems).

II. METHOD DETAILS

A. Transport theory

1. Transport calculation details

In the bottom panel of Fig. 1 we show a schematic diagram of the system under study: a single SiQD surrounded by a SiO₂ matrix and coupled to two semi-infinite metallic electrodes. The external bias voltage V_b applied to the QD is the difference between the left μ_L and right μ_R electrochemical potential of the leads, $\mu_L - \mu_R = qV_b$. In our calculations, we assume that the electrochemical potential of the left lead keeps unchanged while the electrochemical potential of the right lead is raised or lowered, depending on the sign of the applied V_b.

For the sake of comparison, all the systems have the same oxide thickness L of 1.1 nm between the SiQD and the electrodes. This value is in the typical range where tunneling is measured[42] (see the Appendix). The relative dielectric constant of the oxide has been set to 3.9, while the oxide effective mass of electrons and holes has been set to 0.40 m_e and 0.32 m_e, respectively,[43] m_e being the free electron mass. For all the calculations the Fermi energy has been set half between the highest occupied molecular orbital (HOMO) and the lowest unoccupied molecular orbital (LUMO), $E_F = (E_{HOMO} + E_{LUMO})/2$.

2. Theoretical background

We use a transfer Hamiltonian method[40,41] with rate equations to describe the current between the leads, coupled with an elastic scattering region (corresponding to the SiO₂-embedded SiQD), when an external V_b is applied. More details are published elsewhere.[34,35] The interaction between the QD and the electrodes is due to transition rates and capacitive couplings. Effects of the self-charge of the QD are taken into account by solving self-consistently the changes produced by the applied V_b in the local potential U and the DOS of the QD.
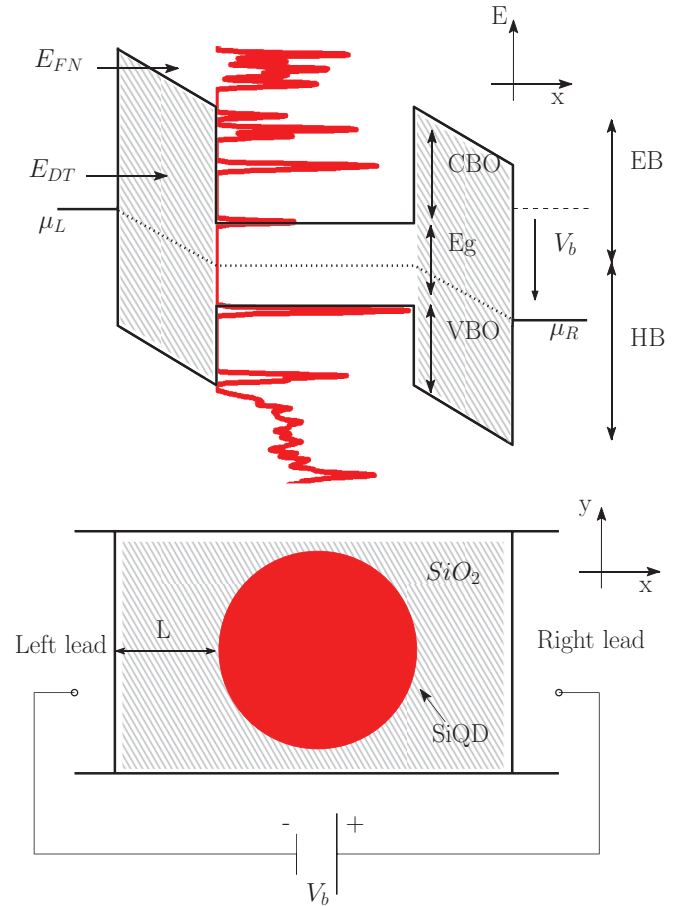

FIG. 1. (Color online) Top: Band diagram (solid black lines) of the system, DOS of the SiQD (solid red line), and Fermi energy E_F (dotted black line) when a bias voltage V_b is applied. The conduction and valence band offset (CBO and VBO) are the difference between the conduction and valence SiO₂ band edge and half the embedded system energy gap E_g, while the electron (hole) barrier EB (HB) is the conduction (valence) SiO₂ band edge with respect to the Fermi energy of the embedded system. The two possible tunnel mechanisms are shown: Fowler-Nordheim (FN) and direct tunnel (DT). Bottom: Schematic diagram of the SiQD surrounded by SiO₂ matrix at a distance L of two semi-infinite leads.

The solution of the Poisson equation for the potential energy $U = -qV$, V being the potential at the QD, is

$$U = U_L + \frac{q^2}{C_{tot}}\Delta N, \tag{1}$$

where U_L is the Laplace solution of the system, C_{tot} is the total capacity, and ΔN is the change in the number of electrons N calculated with respect to the reference number N_0 originally in the QD. The QD charge N is calculated from the DOS ρ_{QD} and the nonequilibrium distribution function n of the QD. A self-consistent solution for the equations of N, n, and U is needed as the effect of the local potential U is taken into account in the QD DOS, $\rho_{QD}(E) \rightarrow \rho_{QD}(E - U)$, as is explained in Ref. 35.

Assuming no inelastic scattering and symmetry in the transmission coefficient,[44] the net current flux between the

two leads is

$$I = \frac{4\pi q}{\hbar} \int \frac{T_L T_R \rho_L \rho_{QD} \rho_R}{T_L \rho_L + T_R \rho_R} (f_L - f_R) dE, \qquad (2)$$

where $T_{L,R}(E)$ are the transmission probabilities between the left lead and the QD and between the QD and the right lead, respectively, $\rho_{L,R,QD}(E)$ are the DOS of each part of the system, and $f_{L,R}(E)$ are the Fermi-Dirac distribution functions of the electrodes.

By assuming ballistic transport we can deal with independent conduction channels for electrons and holes. The current for each carrier type can be calculated from Eq. (2) using the corresponding transmission coefficient and DOS. The total current is the sum of electron and hole currents.

The $\rho_{QD}(E)$ is computed within DFT[45,46] in order to take into account the influence of the surrounding matrix that cannot be described in detail by simpler methods, e.g., by solving the Schrödinger equation of a potential well.[41] The transmission coefficients are calculated using the WKB approximation[36] of Fowler-Nordheim [Eq. (3)] and direct tunnel [Eq. (4)] mechanisms (see the top of Fig. 1), which are the two more relevant tunneling mechanisms in QDs inside dielectric matrices.[47–49] In fact, inelastic scattering has been shown to be unimportant for highly quantum confined systems, such as the ones studied in the present work.[50,51]

$$T(E) = \exp\left\{ -4\frac{\sqrt{2m_{\text{diel}}}}{3\hbar q E_{\text{diel}}} [q\phi_1 - (E - E_{c1})]^{3/2} \right\}, \qquad (3)$$

$$T(E) = \exp\left\{ -4\frac{\sqrt{2m_{\text{diel}}}}{3\hbar q E_{\text{diel}}} [(q\phi_1 - E)^{3/2} - (q\phi_0 - E)^{3/2}] \right\}, \qquad (4)$$

E_{diel} being the electric field in the dielectric barrier, m_{diel} the effective mass inside the dielectric, E_{c1} the conduction band edge of the QD, and ϕ_1 and ϕ_0 the potential barrier height and modified potential barrier height, respectively. Following QC, the energy gap increases with decreasing QD size, so the difference between QD energy levels and matrix band edge also decreases. This implies, *a priori* from Eqs. (3) and (4), an increase of the transmission probability for smaller QDs. However, we will see in Sec. III that other effects contribute to determining the total current.

B. Atomistic models

In the present paper we have carried out *ab initio* calculations of electronic properties for SiQDs of different diameters embedded in SiO$_2$ matrices. Since real sample QDs are characterized by a certain amount of amorphization, especially at small QD sizes,[52,53] we have considered the two opposite ideal cases of perfectly crystalline and completely amorphous systems in order to investigate the effect of the crystallinity on the QD electronic structure and on the confining potential.

1. DFT calculation details

The relaxation of all the systems and the calculation of the DOS have been computed with the DFT code SIESTA.[54,55] Calculations have been performed using norm-conserving Troullier-Martins[56] pseudopotentials with nonlinear core corrections within the local density approximation (LDA) with
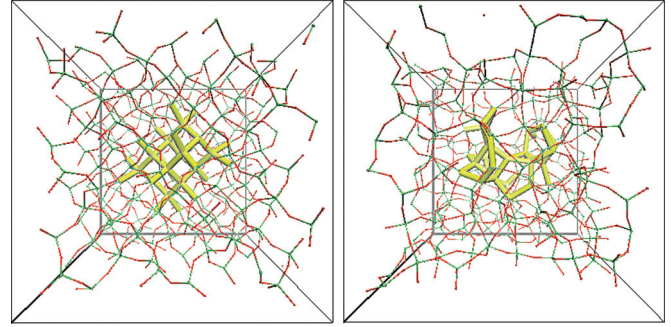

FIG. 2. (Color online) Ground-state structure of the QD of 32 Si atoms in β-cristobalite (left panel) and in silica (right panel). Red (dark gray) spheres are O atoms, green (gray) spheres are Si atoms, and the yellow (gray) thick sticks represent the Si atoms of the QD.

a Ceperley-Alder[57] exchange-correlation potential, as parameterized by Perdew-Zunger.[58] A cutoff of 250 Ry on the electron density and no additional external pressure or stress have been applied. All the calculations have been performed at 0 K temperature with only Γ-point k sampling and standard double-ζ basis set for all the atoms. Atomic positions and cell parameters have been left totally free to move and structural, electrical, and optical properties have been published elsewhere.[16,17]

2. SiO$_2$ matrices and SiQDs

The β-cristobalite SiO$_2$, in the following named c-SiO$_2$, was adopted for the crystalline phase since it is the simplest Si/SiO$_2$ interface due to its diamond-like structure.[59] The glass model for amorphous SiO$_2$, in the following named a-SiO$_2$, was generated using classical molecular-dynamics simulations of quenching from a melt, as described in Ref. 60. The crystalline and amorphous QDs of 32 Si atoms after the ionic relaxation are represented in Fig. 2 for visual comparison.

All the structures have been obtained from a $3 \times 3 \times 3$ supercell Si$_{216}$O$_{432}$ of 21.5 Å of size, by removing all the O atoms inside a cutoff sphere of given radius. According to the number of atoms and to the host matrix, we use the following nomenclature for our systems: c-Si$_{17}$, c-Si$_{32}$, c-Si$_{35}$, and c-Si$_{47}$ for the crystalline SiQDs of 17, 32, 35, and 47 atoms, respectively, and a-Si$_{17}$, a-Si$_{32}$, and a-Si$_{47}$ for the amorphous SiQDs of 17, 32, and 47 atoms, respectively. Using the above methodology, dangling bonds or defects are not present, and all the O atoms at the interface are single bonded to Si atoms of the QD.

After the relaxation, the bond length of Si atoms inside the QD approaches the bulk Si value. For this reason, we propose to use the bulk Si atomic density $\rho_a = N_a/a^3$, with $N_a = 8$ Si atoms in a cubic cell of side $a = 5.43$ Å, to estimate the corresponding final QD radius r_{QD} (which differs from the original cutoff radius). Considering that the QD is formed by n_{Si} Si atoms and n_O interface O atoms:

$$\frac{(n_{Si} + n_O)}{\rho_a} = \frac{4}{3}\pi r_{QD}^3. \qquad (5)$$

The reason for including the interface O atoms in the above definition of the QD radius is that they form states that behave

as part of the QD, and not of the embedding matrix.[61] The behavior of (1) freestanding hydrogenated QDs is different from that of (2) freestanding oxygenated QDs and (3) SiQDs embedded in SiO_2 matrix, due to the absence of O atoms at the QD surface. It is worth noting that while in the first case the QD energy gap is related to the QD diameter by the sole QC,[3] in the second and third case, the surrounding O atoms and the stress induced by the embedding matrix have an important role over the optical and electrical properties. In (3), the band gap is almost completely determined by the barrier provided by the first shell of O atoms, while a competition between the oxidation (that tends to blueshift the absorption spectra) and the strain induced by the embedding matrix (that tends to redshift it) has been observed.[17,62]

Previous works report that in the case of crystalline Si/SiO_2 QD, the HOMO is mainly localized at the interface while the LUMO extends over the entire QD region.[16] It is clearly shown in Ref. [16] that the first shell of the interface O atoms is able to completely trap the QD density charge, thus forming a strong barrier that is responsible of the QC effect.

The generation of the QD inside the a-SiO_2 matrix allows the formation of Si-O-Si bridge bonds at the Si/SiO_2 interface, and the reduction of the embedded system energy gap in all the systems, as shown by previous theoretical studies,[16,64] and in accordance with photoluminescence measurements where the energy gap for QDs around 2.5 nm in diameter was determined to be 1.9 eV for amorphous QDs[65] and 2.7 eV for crystalline ones.[66] Similarly to the crystalline case, HOMO and LUMO states of amorphous systems are localized at the surface of the QD and inside it, respectively.[63]

III. RESULTS AND DISCUSSION

A. Band alignment: SiQD density of states and silica barriers

As shown by Eq. (2) the current depends on the DOS and on the transmission coefficient, the barrier height being the main parameter in tunneling transmission. In order to properly determine these barriers, the DOS of the QD and of the silica matrix were carefully analyzed. Concerning the reliability of our computed DOS results, the Si band gap and other DOS features are in good agreement with other LDA calculations performed using plane waves[20] or a Gaussian basis set.[21]

1. SiQD density of states

To determine the electron states in the SiQD we have used the projected DOS (PDOS) onto SiQD atoms and O atoms of the interface (see Fig. 3). As explained by previous studies,[16,17,19] quantum confinement (QC) of the carriers makes discrete energy states appearing inside the SiO_2 band gap, leading to a reduced gap with respect to bulk SiO_2, and increased with respect to bulk Si. The typical configuration of bulk SiO_2 states is still recognizable far from the band edge, where the influence of the QD is lower.

As explained in the previous section, we have included the interface O atoms in the transport calculation because they strongly influence the QD optical and electrical properties.[19,20,23,67] Previous works[17] support the idea of two mechanisms, QC and chemical environment, in the determination of the embedded system energy gap (E_g) with respect to that of bulk Si: While the E_g of large QD (>3 nm) can be approximated as purely QC driven, for small QD the
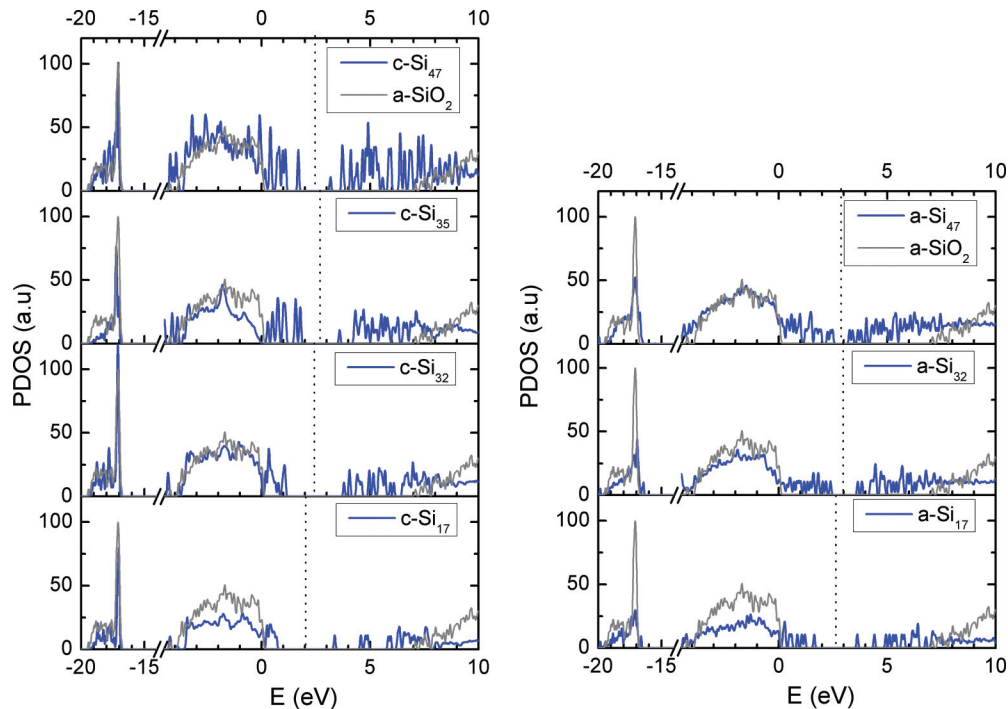

FIG. 3. (Color online) PDOS of the crystalline and amorphous SiQDs (blue line) compared to a-SiO_2 DOS (gray line). The valence band maximum of silica defines the zero energy in all the cases. The Fermi energy is located in the middle of the HOMO-LUMO band gap of the embedded systems (black dotted line).

TABLE I. Corrected conduction and valence band offsets (CBO and VBO) of QDs with respect to electron (EB) and hole (HB) barrier, QD band gaps (E_g), QD diameters (d), and volume variation (ΔV) of each system.

	d (nm)	ΔV (%)	E_g (eV)	CBO (eV)	VBO (eV)	EB (eV)	HB (eV)
c-Si₁₇	1.27	−16.19	2.69	2.93	2.69	4.27	4.03
c-Si₃₂	1.50	−21.05	2.74	2.49	3.06	3.86	4.43
c-Si₃₅	1.39	−23.90	1.82	2.69	3.78	3.60	4.69
c-Si₄₇	1.60	−14.58	1.48	3.12	3.69	3.86	4.43
a-Si₁₇	1.24	−9.56	1.98	2.67	3.64	3.66	4.63
a-Si₃₂	1.45	−4.68	1.25	2.66	4.39	3.28	5.01
a-Si₄₇	1.59	−8.80	0.79	3.03	4.49	3.42	4.88

chemistry at the interface rules over the other mechanisms and such approximation cannot hold anymore.[79]

For the sake of comparison with the SiQD PDOS, the total DOS of a-SiO₂ is also shown in Fig. 3, where the zero of energies has been set at the valence band edge of the silica. Clearly, the number of states depends on QD size, with bigger systems having more states inside the silica gap.[39] The computed E_g for a-SiO₂ and bulk Si are 7.1 eV and 0.6 eV, respectively, in agreement with other calculations,[68] and smaller than the experimental values (9.0 eV for a-SiO₂[69] and 1.1 eV for bulk Si).

It is well known that Kohn-Sham eigenvalues give an underestimated E_g that can be improved by quasiparticle excitations.[77,78] However, while the latter correction is noticeable in bulk materials (i.e., Si, SiO₂), in strongly confined systems the enhanced excitonic interaction is known to reduce E_g of about same amount. As a consequence, the E_g of QDs computed by DFT-LDA is, at the end, similar to those obtained by more sophisticated many-body methods.[16] For the above reason, in the case of a small embedded QD, one deals with "correct" E_g values (determined by QD states), but "uncorrect" band offsets due to the systematic error in the SiO₂-related energy values. Following the above assumption, we have applied a constant correction to the calculated valence and conduction band offsets (see below), and not to E_g. We note that our uncorrected values of band offsets match those of other works,[22] that have been previously used to investigate charge-carrier transport in SiQDs by hopping mechanisms.[70]

2. Silica barriers: Band offset, band gap, and band edge

The interface between SiQD and SiO₂ clearly forms a type-I heterojunction, like the well-investigated interface between these two materials in bulk or planar systems.[68,71–75] In the case of a Si/SiO₂ slab calculation in the bulk limit, we have obtained a valence band offset (VBO) and conduction band offset (CBO) of 2.6 eV and 3.9 eV, respectively, to be compared with the experimental values of 4.6 eV (VBO) and 3.1 eV (CBO).[4,11]

As reported in other studies through energy band localization[61] or projected band edges on each atom,[22] the presence of QC makes VBO and CBO between SiQDs and SiO₂ significantly differ from the values of bulk or planar systems. Like previous works,[76] we have aligned the PDOS using the strong peak of the a-SiO₂ DOS as reference, located at about −17 eV, which is well observable in all the studied

structures (see Fig. 3). Then, we have obtained the VBO as the difference between the QD HOMO and silica HOMO, and the CBO as the difference between the silica LUMO and the QD LUMO. We also define the electron barrier (EB) as the difference between the LUMO of silica and E_F, and the hole barrier (HB) as the difference between E_F and the HOMO of silica. Finally, to compensate the above-discussed DFT limitations, we have applied a correction of 2.0 eV to VBO and HB values, and of −0.8 eV to CBO and EB values. As our QD size range is small, we use the same energy shift for all the data.

Since the embedded QD induces a deformation of the surrounding matrix, the c-SiO₂ tends to lose its symmetry after the embedding. This makes the c-SiO₂ matrix behave as the amorphous one after the relaxation. For this reason we have used the DOS of the a-SiO₂ matrix as reference also for all crystalline structures.

In Table I we report for all the structures the corrected values of E_g, CBO, VBO, EB, and HB. The diameter d of the QD and the volume variation with respect to the unrelaxed original structure, V(c-SiO₂) = 11.04 nm³ and V(a-SiO₂) = 9.10 nm³, are also presented.

From the calculations, two main trends of the band offset emerge: one related to the QD size and the other related to the amorphization level, as has been shown in recent experiments of the band alignment in SiQDs between 1.9 and 4.3 nm embedded in a SiO₂ matrix.[11,12] From Fig. 4 (upper panel) we can observe that band offset increases with the QD size (more pronounced for valence band, VB, than for conduction band, CB), consistently with the planar value corresponding to very large diameter. This trend has been previously reported by Wolkin *et al.*[67] and Li *et al.*,[76] and supported by soft x-ray spectroscopy measurements[80] and photoionization and capacitance spectroscopy measurements[12] of small embedded SiQDs. Thus, we observe an overall decrease of E_g with the QD size, as dictated by QC. Li *et al.*[76] explain the different behavior of CB and VB by analyzing the spatial distribution of the HOMO and LUMO states, and they explained the sensitivity of the HOMO state to the surrounding matrix by considering its localization at the QD interface. Conversely, since the LUMO state extends over the whole QD, differences in the surrounding matrix have poor effects on it.

Furthermore, Fig. 4 (upper panel) reports crystalline VBOs lower than the amorphous counterparts for QDs of similar diameter. Instead, CBOs have no clear trend between different embedding matrices. In a previous work we showed that, for the Si₃₂ QD, the crystalline system has smaller band offsets with respect to the amorphous one, since in the latter case
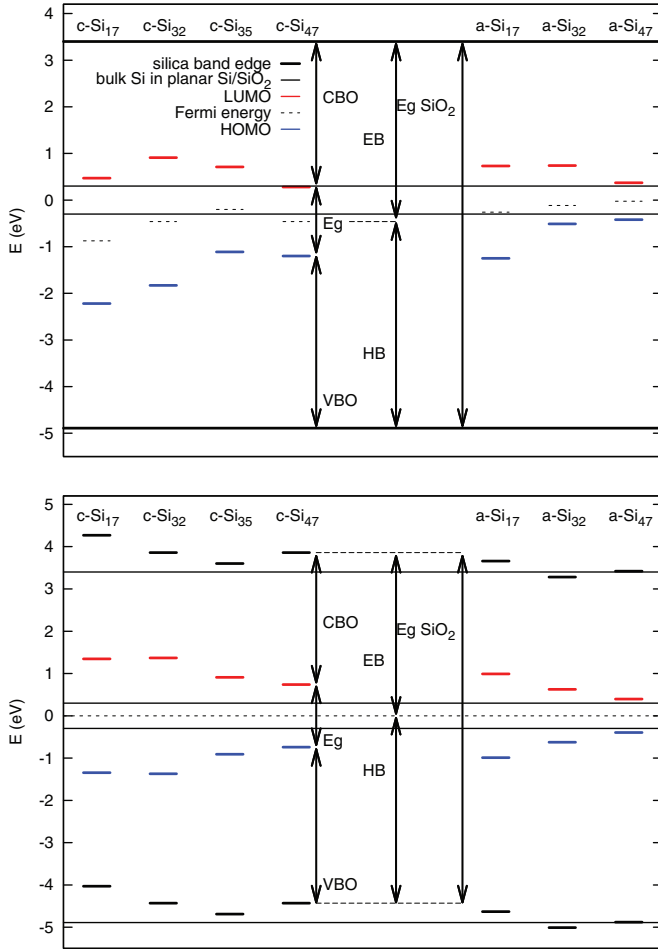
FIG. 4. (Color online) Energy band profile of the QDs (HOMO in blue lines and LUMO in red lines): (top) with respect to the same silica band edges (solid black lines), and (bottom) with respect to the same Fermi energy (black dot line). Fermi energy for each system is placed in the middle of the HOMO-LUMO energy gap E_g. The value for bulk Si in planar Si/SiO$_2$ interface (thin black lines) with the same computational parameters used in this work is shown for comparison.

conduction states progressively move from the QD to the matrix for increasing energy, and become pure matrix states only at 5 eV above the LUMO.[61]

In conclusion, we can state that the VBO (and the CBO in a lower strength) generally increases with the QD diameter, thus expecting higher current for smaller QDs. Besides, E_g determines the conductivity threshold, and it decreases with diameter. Thus, while large QDs have high barriers (i.e., low transmission probability), at high V_b they might present higher currents, as a large number of states enters the conduction window (i.e., between μ_L and μ_R) and are available to the carriers.

To further understand the implication of both mechanisms we show in Fig. 4 (bottom panel) an alternative representation of the energy band profile in which the Fermi energy of all the systems has been aligned. We observe that the HB and EB, i.e., the sum of band offset and half the band gap of the embedded system, collects both the above-discussed trends with the QD diameter: The band offset increases with the QD size giving lower transmission probability whereas E_g decreases being
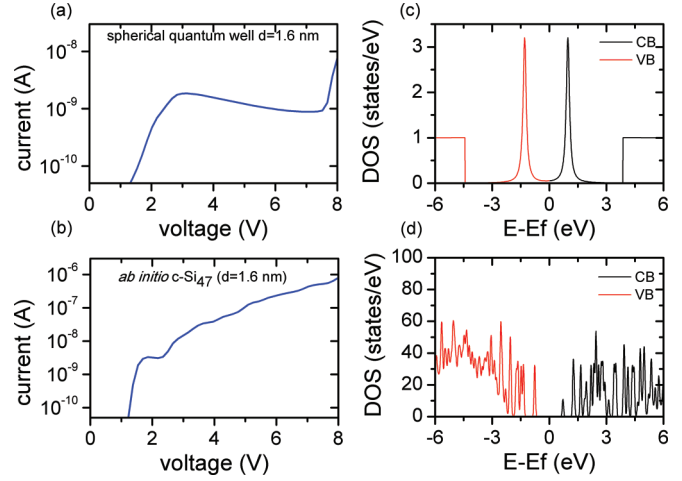

FIG. 5. (Color online) Comparison between (a) total current (electrons + holes) computed with DOS extracted from the solution of a particle in a spherical quantum well and (b) calculated by *ab initio* DFT. Comparison between (c) DOS by spherical quantum well and (d) by *ab initio* DFT. Fermi energy is set to zero and located in the middle of the HOMO-LUMO band gap.

more states inside the conduction window. We have reported in Sec. III B 1 the implication of this parameter on the total current.

B. Description of *I-V* characteristics

In this section we present the computed electron and hole *I-V* characteristics for all the structures. We only show positive voltages in our computed *I-V* characteristics because of the symmetry related to the same tunneling distance between the electrodes and the QD.

In a simpler way with respect to the method used in this paper, the most common way to model a QD is by using a spherical[36] or cubic[39] potential well, with a width corresponding to the QD diameter, and using the planar Si/SiO$_2$ value for band offsets.[9,36,39] Such approach leads to the $1/d^\alpha$ relationship between the E_g and diameter d, with $\alpha = 2$ in the case of an infinite barrier.[3,81] In Fig. 5 we report a comparison between transport properties obtained with DOS calculated by DFT or by a spherical quantum well with the same QD radius and barrier values. Although modeling the QD as a quantum well may be convenient to generate QDs of arbitrary size, in particular large QDs which are difficult to treat at the *ab initio* level, only the atomistic methods enable the description of interface states, as clearly shown in Fig. 5(d) by the quasicontinuous DOS.

In Fig. 6 the computed *I-V* characteristic (left panel) and the differential conductance dI/dV (right panel) for the c-Si$_{47}$ ($d = 1.6$ nm) are compared to the experimental results of Ref. 4 (layers with QDs of about 4 nm of diameter in a parallel configuration) and of Ref. 66 (samples of QDs with diameter range from 2 to 10 nm). As we can see, our results qualitatively match the experimental ones, validating the methodology and the employed models. Both experimental and theoretical *I-V* characteristics show a diode behavior, with currents peaked at 1.5 eV and 1.8 eV, respectively, related to the QD DOS. The theoretical curve presents a threshold voltage at about
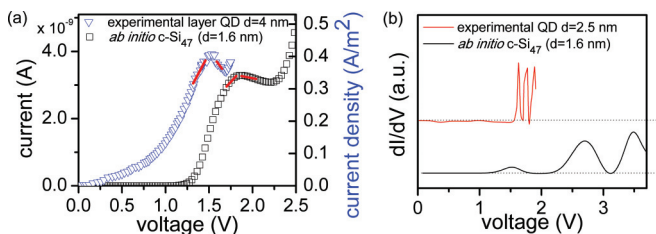
FIG. 6. (Color online) (a) Comparison between the (blue triangles) experimental *I-V* characteristic of a layer of QDs of diameters around 4 nm (Ref. 4) and (black squares) of the c-Si$_{47}$ QD from present work ($d = 1.6$ nm). Red lines indicate the slope of the peak sides (see text). (b) Comparison between an experimental dI/dV curve (red line) of one QD of diameter around 2.5 nm (Ref. 66) and (black line) of the c-Si$_{47}$ QD from present work ($d = 1.6$ nm).

1.5 V related to the E_g of the system, not visible in the experimental curve. At low bias, the difference between the experimental and theoretical curve should be related to the contribution of impurities. Since our structures are defect free we have a sharp increase of the current in the proximity of the QD gap, while impurities in the experimental sample permit a current flow also at low voltage. Instead, at higher voltage, i.e., when bulk transport of the QD dominates over defects, we recover a correspondence between the curves. In addition, the experimental samples are made by a large ensemble of different QDs, making a direct comparison with our case not straightforward, especially at low voltage. The proportion between the two slopes characterizing the main peak is similar [see the red lines in Fig. 6(a)], being 3.7 ± 0.4 for the DFT curve and 3.1 ± 0.7 for the experimental one. Both dI/dV curves show peaks that are related to the QD discrete energy states. The difference in the conduction gaps is related to the difference in capacitance values and QD diameter. Furthermore, since QDs in parallel configuration act as independent channels, i.e., the total current is given by the sum of the individual QD currents,[34] our results can in principle be compared to experimental measurements made on QD layers in parallel.[4]

The discrete nature of the QD states and the quasicontinuous DOS of interface atoms directly reflects on the current, as reported in Fig. 7. A peak in the current appears whenever an energy level of the QD, or conductive level, enters the conduction window. The regions in which the current decreases with the voltage, known as negative differential resistance (NDR), appear because the potential well of the QD is modified by the external V_b. Thus, at high V_b, the charge accumulated on a conductive energy level decreases with increasing V_b, since the ratio between the incoming and outcoming transmission coefficient decreases with V_b.[26] NDR almost does not appear in the largest QD [Fig. 7(b)] due to a reduced presence of isolated peaks in the DOS, as reported in Figs. 7(e)–7(f).

The dI/dV curve is usually employed experimentally to extract the single-particle energy spectrum of the QD,[5,66,82] since a peak in dI/dV appears whenever an energy level of the QD is aligned with the electrochemical potential of one of the electrodes. Therefore, the possibility of theoretically predicting the dI/dV curve from our calculations opens the possibility of accurately describing the transport in these kinds
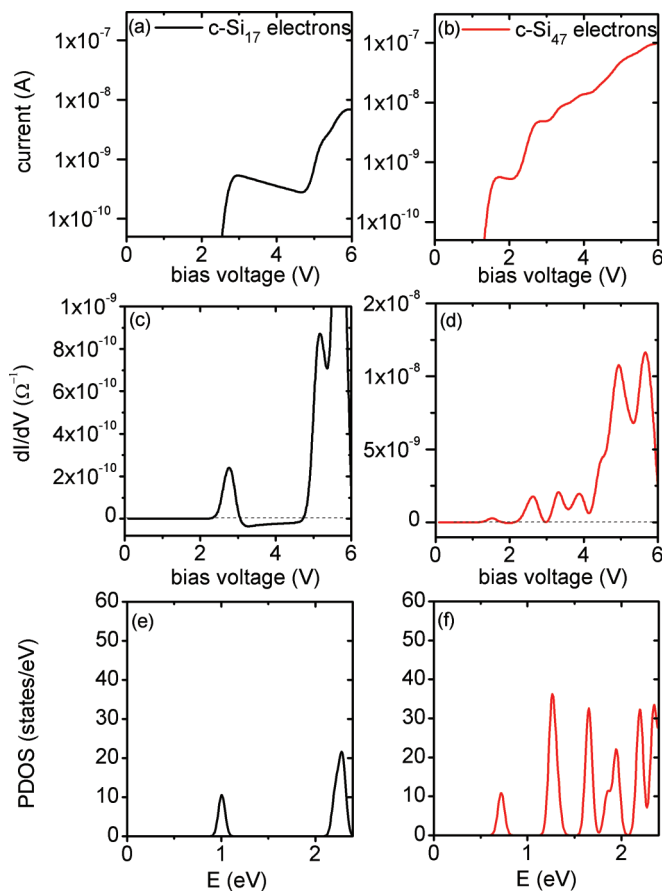

FIG. 7. (Color online) Comparison of the smallest (c-Si$_{17}$ in black) and highest (c-Si$_{47}$ in red) system current [(a) and (b)], differential conductance [(c) and (d)], and PDOS [(e) and (f)].

of complex systems[83] and of reducing its related instabilities, such as the current temporal self-oscillation in superlattices.[26]

The first peak in the dI/dV curve marks the threshold voltage above which carriers can tunnel inside the dot, related to the fundamental energy gap E_g of the system. In Fig. 7 we can see that this peak occurs at a V_b nearly twice the energy of the corresponding peak in the DOS. This is related to the fact that the Laplace solution U_L of one QD and equal capacitance couplings for both electrodes is $U_L = -qV_b/2$, and, since the Poisson term is small, the potential V inside the QD [Eq. (1)] becomes nearly half the bias voltage V_b.[35]

Clearly, the higher dI/dV values of c-Si$_{47}$ are connected to the faster increase of the current with V_b. Conversely, the sharp dI/dV curve and negative values for c-Si$_{17}$ are associated with the resonant peaks of the spectrum and to the NDR, respectively.

1. Electron transport

As already mentioned in Sec. III A2, CBO does not vary substantially in our systems, and therefore electron current is primarily determined by E_g and by the position and number of the QD states (see Fig. 8). Thus, since the smallest QDs (c-Si$_{17}$ and a-Si$_{17}$) present the highest E_g and the smallest DOS, they produce the lowest electron currents. For the same reason, we observe a clear trend of increasing electron current with the QD size, although the range of diameters presented in this paper is
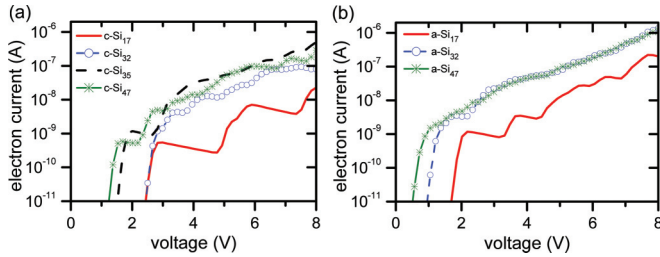
FIG. 8. (Color online) Electron *I-V* characteristic for (a) crystalline systems and (b) amorphous systems.

quite limited to permit visible differences between the largest QDs, especially in the case of amorphous structures. Besides, for QDs with similar E_g values, such as c-Si$_{32}$ and c-Si$_{17}$, the largest current is achieved by the one with the smallest CBO, as expected.

2. Hole transport

From Fig. 9 we note that hole transport radically differs from electron transport. For example, the small VBO values of c-Si$_{17}$ and a-Si$_{17}$ rule over their large E_g, and although the larger V_b threshold with respect to the other systems, the low hole barriers enhance the hole transport in these small systems. For the other structures, the influence of VBO and E_g are mixed, with no clear trend with the QD size. Besides, since HB sums up the opposite trends of VBO and E_g with the QD size (see Fig. 4), a correlation of HB with the hole current is observable. Systems that have different VBO and E_g, such as c-Si$_{32}$ and c-Si$_{47}$ or a-Si$_{17}$ and a-Si$_{47}$, have a similar current for high bias voltages due to their similar HB values. This is clearly visible for the c-Si$_{47}$, which is the first system to show current among crystalline cases, and has a rather larger VBO than (for example) c-Si$_{32}$. Therefore, when V_b approaches the threshold value of the other systems, the c-Si$_{47}$ current is supported by several states inside the conduction window, and the final currents become comparable. In conclusion we can expect, *a priori*, from the tendency of HB to increase with SiQD size up to the theoretical value (see the bottom of Fig. 4), an enhancement of hole current in small systems. However, in real big systems, the strong DOS and small E_g may possibly overcome the effect of a large HB in small QD. This point should be further investigated next, when the present computational limits for these systems will be improved.
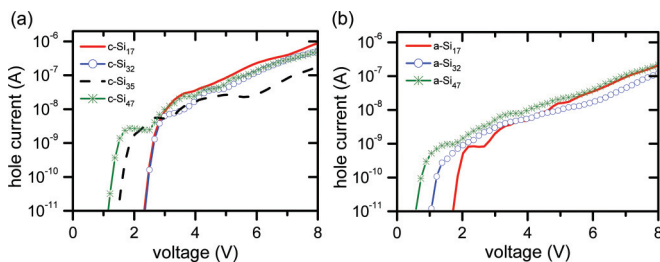

FIG. 9. (Color online) Hole *I-V* characteristic for (a) crystalline systems and (b) amorphous systems.
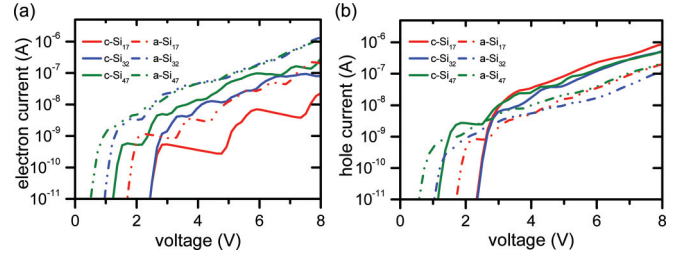

FIG. 10. (Color online) Comparison of (a) electron and (b) hole transport for crystalline and amorphous systems.

3. Crystalline and amorphous matrices

To investigate the influence of disorder in the transport properties we have reported all the electron (left panel) and hole (right panel) *I-V* characteristics in Fig. 10. At first we note that, for what is discussed above and for the tendency of amorphization to reduce E_g, the higher electron currents are produced by the amorphous systems. Also, the reduced EB in the amorphous QDs helps in enhancing the electron current in these systems. From the other side, the reduced HB in the crystalline QDs favors the hole transport in the crystalline systems.

IV. CONCLUSIONS

We have investigated the dependence of electron and hole transport and of electronic properties on the embedded SiQD size using DFT calculations for the DOS, a transfer Hamiltonian approach for the expression of the current, and a WKB approximation for the expressions of the transmission coefficients. In the case QDs of a few nanometers, strong nonplanar interfaces between Si and SiO$_2$ require a different treatment with respect to common planar Si/SiO$_2$ devices. We have shown that for small QD size the quantum well models cannot describe accurately DOS and band offset, because of the large contribution of interface states. In this regime an *ab initio* approach is necessary to realistically take into account the atomistic detail at the interface.

Electronic transport is determined by a competition between transmission probability (dependent on the silica barrier height or band offset), available states inside the silica barrier (related to the QD DOS), and conduction gap (dependent on the embedded system energy gap E_g). Generally speaking, when the QD diameter increases, the VBO increases (CBO has a weaker dependence) while E_g decreases, with some fluctuations related to the oxidation degree at the interface and to the strain induced by the embedding matrix. Besides, the number of states inside the barrier increases with the QD size. Thus, when the diameter increases, the higher DOS and lower E_g enhances the current, whereas the higher band offset reduces it. Since electron barriers (EB) and hole barriers (HB) (i.e., the sum of the band offset and half the energy gap) gather the opposite trend of band offset and E_g with the QD size, we propose to use them as a single parameter to characterize the electronic transport. In fact, lower EB and HB correspond in general to higher currents, with asymmetric behavior for electron and holes.

Electron transport is enhanced in big systems due to the larger DOS and because CBO does not vary significantly.

Therefore EB follows E_g, being lower for bigger systems. Conversely, hole transport is enhanced in the smallest systems because of the reduced VBO, although no clear trend with the QD size is observed. Besides, we have evidenced a direct relationship between hole transport and HB, the latter increasing with the QD size up to the planar value.

Concerning the systems morphology, amorphous QDs present higher electron current than crystalline ones for a given QD size because of their smaller E_g. Hole transport, however, is enhanced for crystalline systems due to the much smaller HB, supporting the idea of an efficient electron confinement in crystalline QDs.

In conclusion, our calculations show that the transport properties of small Si/SiO$_2$ QDs are extremely sensitive to the microstructure of the QD/SiO$_2$ interface. In practice, this means that the design and fabrication of devices based on small QDs with predictable properties requires a fine control of these properties that go far beyond the mere control of the QD diameter.

APPENDIX: FOWLER-NORDHEIM PARAMETERS

Beside the relative variation of the current with the QD configuration, it is useful to determine the current relative to the pure SiO$_2$, and the corresponding parameters of the FN model, in order to provide a reference for the embedding material. In Fig. 11 we report the calculation of transport through a SiO$_2$ layer with a thickness $L = 3.8$ nm, corresponding to size of the c-Si$_{47}$ QD encompassed by the two 1.1 nm SiO$_2$ slices. By fitting the *I-V* curve with the FN expression[84]

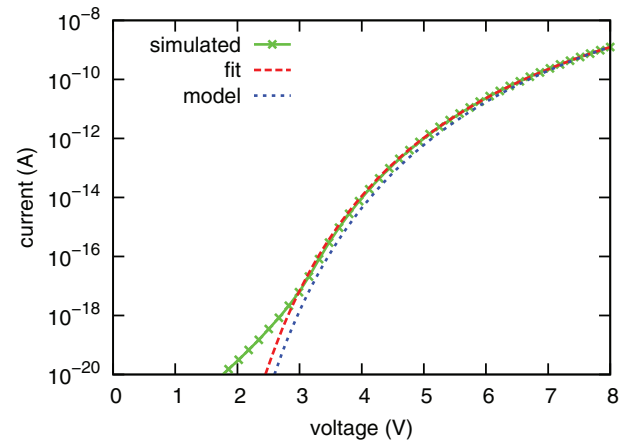$$I = \hat{C} V^2 e^{-\hat{\beta}/V}, \tag{A1}$$

FIG. 11. (Color online) Calculated *I-V* curve of a SiO$_2$ layer (solid line with symbols) with the corresponding FN fit of Eq. (A1) (dashed line), and the same FN function parametrized by Eq. (A4) (dotted line).

we obtain $\hat{\beta} = 81.9 \pm 0.1$ V and $\hat{C} = 5.4 \times 10^5 \pm 0.1 \times 10^5$ A/MV^2 (dashed curve of Fig. 11).

Usually in experiments the transport is expressed in terms of the current density

$$J = C E^2 e^{-\beta/E}, \tag{A2}$$

in which E is the applied field. Equations (A1) and (A2) are related by

$$\beta = \hat{\beta}/L, \quad C = \hat{C} L^2/S, \tag{A3}$$

in which S is the cross-sectional area of the scattering region (the geometrical factor L^2/S is implicitly assumed equal to unity in our simulations; i.e., $C = \hat{C}$).

From Eqs. (A1)–(A3) we obtain $\beta = 215.6 \pm 0.2$ MV/cm, well matching the literature values.[84,85] Moreover, by using the direct expressions[84]

$$\beta = \frac{4\phi^{3/2}\sqrt{2m_{ox}}}{3q\hbar}, \quad C = \frac{q^3 m_e}{(16\pi^2\hbar\phi m_{ox})} \tag{A4}$$

with the computational parameters used in this work, i.e., $m_{ox} = 0.4\ m_e$ and $\phi_0 = 3.1$ eV, we obtain $\beta = 235.7$ MV/cm and $C = 12.4 \times 10^5$ A/MV^2. The plot of Eq. (A1) parametrized by the latter values is reported in Fig. 11 (dotted curve). The discrepancy between the computed and the parametrized curves at low voltage should be related to direct tunneling, taken into account in the simulation beside the FN process.

*nuriagarcia@ub.edu

[1] W. Shockley and H. J. Queisser, J. Appl. Phys. **32**, 510 (1961).

[2] C. H. Henry, J. Appl. Phys. **51**, 4494 (1980).

[3] J. P. Proot, C. Delerue, and G. Allan, Appl. Phys. Lett. **61**, 1948 (1992).

[4] G. Conibeer *et al.*, Thin Solid Films **511-512**, 654 (2006).

[5] U. Meirav and E. B. Foxman, Semicond. Sci. Technol. **11**, 255 (1996).

[6] S. Tiwari, F. Rana, K. Chan, L. Shi, and H. Hanafi, Appl. Phys. Lett. **69**, 1232 (1996).

[7] I. Perez-Wurfl, X. Hao, A. Gentle, D. H. Kim, G. Conibeer, and M. A. Green, Appl. Phys. Lett. **95**, 153506 (2009).

[8] G. Conibeer *et al.*, Thin Solid Films **516**, 6748 (2008).

[9] J. Carreras, O. Jambois, S. Lombardo, and B. Garrido, Nanotechnology **20**, 155201 (2009).

[10] O. Jambois, J. Carreras, A. Pérez-Rodríguez, B. Garrido, C. Bonafos, S. Schamm, and G. Ben Assayag, Appl. Phys. Lett. **91**, 211105 (2007).

[11] G. Seguini, S. Schamm-Chardon, P. Pellegrino, and M. Perego, Appl. Phys. Lett. **99**, 082107 (2011).

[12] G. Seguini, C. Castro, S. Schamm-Chardon, G. BenAssayag, P. Pellegrino, and M. Perego, Appl. Phys. Lett. **103**, 023103 (2013).

[13] E. G. Barbagiovanni, L. V. Goncharova, and P. J. Simpson, Phys. Rev. B **83**, 035112 (2011).

[14] S. Godefroo, M. Hayne, M. Jivanescu, A. Stesmans, M. Zacharias, O. I. Lebedev, G. van Tendeloo, and V. V. Moshchalkov, Nat. Nanotechnol. **3**, 174 (2008).

[15] L. Pavesi, L. D. Negro, C. Mazzoleni, G. Franzò, and F. Priolo, Nature (London) **408**, 440 (2000).

[16] R. Guerra, I. Marri, R. Magri, L. Martin-Samos, O. Pulci, E. Degoli, and S. Ossicini, Phys. Rev. B **79**, 155320 (2009).

[17] R. Guerra, E. Degoli, and S. Ossicini, Phys. Rev. B **80**, 155332 (2009).

[18] R. Guerra and S. Ossicini, Phys. Rev. B **81**, 245307 (2010).

[19] M. Luppi and S. Ossicini, Phys. Rev. B **71**, 035340 (2005).

[20] N. Daldosso *et al.*, Phys. Rev. B **68**, 085327 (2003).

[21] N. B. Nguyen, C. Dufour, and S. Petit, J. Phys.: Condens. Matter **20**, 455209 (2008).

[22] K. Seino, F. Bechstedt, and P. Kroll, Phys. Rev. B **82**, 085320 (2010).

[23] K. Seino, F. Bechstedt, and P. Kroll, Nanotechnology **20**, 135702 (2009).

[24] J. B. Barner and S. T. Ruggiero, Phys. Rev. Lett. **59**, 807 (1987).

[25] J. Weis, J. Haug, K. V. Klitzing, and K. Ploog, Phys. Rev. Lett. **71**, 4019 (1993).

[26] S. D. Wang, Z. Z. Sun, N. Cue, H. Q. Xu, and X. R. Wang, Phys. Rev. B **65**, 125307 (2002).

[27] W. G. van der Wiel, S. De Franceschi, T. Fujisawa, J. M. Elzerman, S. Tarucha, and L. P. Kouwenhoven, Science **289**, 2105 (2000).

[28] Z. Z. Sun, R. Q. Zhang, W. Fan, and X. R. Wang, J. Appl. Phys. **105**, 043706 (2009).

[29] A. Levy Yeyati, A. Martin-Rodero, and F. Flores, Phys. Rev. Lett. **71**, 2991 (1993).

[30] Y. Meir, N. S. Wingreen, and P. A. Lee, Phys. Rev. Lett. **66**, 3048 (1991).

[31] Y. Han, W. Gong, H. Wu, and G. Wei, Physica B **404**, 2001 (2009).

[32] U. Aeberhard, Opt. Quant. Electron **44**, 133 (2012).

[33] E. Taranko, M. Wiertel, and R. Taranko, J. Appl. Phys. **111**, 023711 (2012).

[34] S. Illera, N. Garcia-Castello, J. D. Prades, and A. Cirera, J. Appl. Phys. **112**, 093701 (2012).

[35] S. Illera, J. D. Prades, A. Cirera, and A. Cornet, Europhys. Lett. **98**, 17003 (2012).

[36] S. Illera, J. D. Prades, A. Cirera, and A. Cornet, arXiv:1207.5513.

[37] C. Flynn, D. König, I. Perez-Wurfl, M. A. Green, and G. Conibeer, Semicond. Sci. Technol. **25**, 045011 (2010).

[38] C. Jiang and M. A. Green, J. Appl. Phys. **99**, 114902 (2006).

[39] P. Löper, R. Müller, D. Hiller, T. Barthel, E. Malguth, S. Janz, J. C. Goldschmidt, M. Hermle, and M. Zacharias, Phys. Rev. B **84**, 195317 (2011).

[40] M. C. Payne, J. Phys. C **19**, 1145 (1986).

[41] M. Passoni and C. E. Bottani, Phys. Rev. B **76**, 115404 (2007).

[42] J. Halbritter, G. Repphun, S. Vinzelberg, G. Staikov, and W. J. Lorenz, Electrochim. Acta **40**, 1385 (1995).

[43] W. C. Lee and C. Hu, IEEE Trans. Electron Devices **48**, 1366 (2001).

[44] S. Datta, in *Electronic Transport in Mesoscopic Systems*, edited by H. Ahmad, M. Pepper, and A. Broers (The Press Syndicate of the University of Cambridge, Cambridge, 1995), Vol. 3.

[45] P. Hohenberg and W. Kohn, Phys. Rev. **136**, B864 (1964).

[46] W. Kohn and L. J. Sham, Phys. Rev. **140**, A1133 (1965).

[47] D. J. DiMaria, D. W. Dong, C. Falcony, T. N. Theis, J. R. Kirtley, J. C. Tsang, D. R. Young, and F. L. Pesavento, J. Appl. Phys. **54**, 5801 (1983).

[48] I. Balberg, J. Appl. Phys. **110**, 061301 (2011).

[49] G. Pucker, E. Serra, and Y. Jestin, in *Quantum Dots—A Variety of New Applications*, edited by A. Al-Ahmadi (InTech, Croatia, 2012), Chap. 4.

[50] L. Rota, F. Rossi, S. M. Goodnick, P. Lugli, E. Molinari, and W. Porod, Phys. Rev. B **47**, 1632 (1993).

[51] L. E. Henrickson, A. J. Glick, G. W. Bryant, and D. F. Barbe, Phys. Rev. B **50**, 4482 (1994).

[52] F. Gourbilleau, C. Ternon, D. Maestre, O. Palais, and C. Dufour, J. Appl. Phys. **106**, 013501 (2009).

[53] H. Rinnert, M. Vergnat, and A. Burneau, J. Appl. Phys. **89**, 237 (2001).

[54] J. M. Soler, E. Artacho, J. D. Gale, A. García, J. Junquera, P. Ordejón, and D. Sánchez-Portal, J. Phys.: Condens. Matter **14**, 2745 (2002).

[55] P. Ordejón, E. Artacho, and J. M. Soler, Phys. Rev. B **53**, R10441 (1996).

[56] N. Troullier and J. L. Martins, Phys. Rev. B **43**, 8861 (1991).

[57] D. M. Ceperley and B. J. Alder, Phys. Rev. Lett. **45**, 566 (1980).

[58] J. P. Perdew and A. Zunger, Phys. Rev. B **23**, 5048 (1981).

[59] H. Kageshima and K. Shiraishi, in *Proceedings of the 23rd International Conference on the Physics of Semiconductors*, edited by M. Scheffer and R. Zimmermann (World Scientific, Singapore, 1996), p. 903.

[60] L. Martin-Samos, Y. Limoge, J.-P. Crocombette, G. Roma, N. Richard, E. Anglada, and E. Artacho, Phys. Rev. B **71**, 014116 (2005).

[61] R. Guerra, E. Degoli, M. Marsili, O. Pulci, and S. Ossicini, Phys. Status Solidi B **247**, 2113 (2010).

[62] K. Küsová *et al.*, Appl. Phys. Lett. **101**, 143101 (2012).

[63] P. Kroll and H. J. Schulte, Phys. Status Solidi B **243**, R47 (2006).

[64] M. G. Mavros, D. A. Micha, and D. S. Kilin, J. Chem. Phys. C **115**, 19529 (2011).

[65] N. Park, T. Kim, and S. Park, Appl. Phys. Lett. **78**, 2575 (2001).

[66] B. Zaknoon and G. Bahir, Nano Lett. **8**, 1689 (2008).

[67] M. V. Wolkin, J. Jorne, P. M. Fauchet, G. Allan, and C. Delerue, Phys. Rev. Lett. **82**, 197 (1999).

[68] M. Ribeiro, L. R. C. Fonseca, and L. G. Ferreira, Phys. Rev. B **79**, 241312 (2009).

[69] S. Miyazaki, H. Nishimura, M. Fukuda, L. Ley, and J. Ristein, Appl. Surf. Sci. **113-114**, 585 (1997).

[70] K. Seino, F. Bechstedt, and P. Kroll, Phys. Rev. B **86**, 075312 (2012).

[71] K. Seino, J. M. Wagner, and F. Bechstedt, Appl. Phys. Lett. **90**, 253109 (2007).

[72] T. Yamasaki, C. Kaneta, T. Uchiyama, T. Uda, and K. Terakura, Phys. Rev. B **63**, 115314 (2001).

[73] R. Shaltaf, G.-M. Rignanese, X. Gonze, F. Giustino, and A. Pasquarello, Phys. Rev. Lett. **100**, 186401 (2008).

[74] A. Alkauskas, P. Broqvist, F. Devynck, and A. Pasquarello, Phys. Rev. Lett. **101**, 106802 (2008).

[75] S. Markov, P. V. Sushko, S. Roy, C. Fiegna, E. Sangiorgi, A. L. Shluger, and A. Asenov, Phys. Status Solidi A **205**, 1290 (2008).

[76] T. Li, F. Gygi, and G. Galli, Phys. Rev. Lett. **107**, 206805 (2011).

[77] R. Del Sole, L. Reining, and R. W. Godby, Phys. Rev. B **49**, 8024 (1994).

[78] E. K. Chang, M. Rohlfing, and S. G. Louie, Phys. Rev. Lett. **85**, 2613 (2000).

[79] R. Guerra, F. Cigarini, and S. Ossicini, J. Appl. Phys **113**, 143505 (2013).

[80] A. Zimina, S. Eisebitt, W. Eberhardt, J. Heitmann, and M. Zacharias, Appl. Phys. Lett. **88**, 163103 (2006).

[81] O. Bisi, S. Ossicini, and L. Pavesi, Surf. Sci. Rep. **38**, 1 (2000).

[82] L. P. Kouwenhoven, C. M. Marcus, P. L. Mceuen, S. Tarucha, R. M. Westervelt, and N. S. Windgren, in *Electron Transport in Quantum Dots*, edited by L. L. Sohn, L. P. Kouwenhoven, and G. Schön (Kluwer, New York, 1997), pp. 105–214.

[83] See page 269 of Ref. 5 for a more detailed description.

[84] N. M. Ravindra and J. Zhao, Smart Mater. Struct. **1**, 197 (1992).

[85] N. Harabech, R. Bouchakour, P. Canet, P. Pannier, and J. P. Sorbier, in *Proceedings of the 2000 IEEE International Symposium on Circuits and Systems, ISCAS, Geneva*, Vol. 2 (IEEE, Piscataway, 2000), pp. 441–444.